AN AMORPHOUS SELENIUM LIQUID CRYSTAL LIGHT VALVE FOR X-RAY IMAGING

Pia-Krista Rieppo, Birendra Bahadur* and J.A. Rowlands
University of Toronto, Sunnybrook Health Science Centre
Toronto, Ontario, M4N 3M5, Canada

* Litton Systems Canada, 25 City View Drive, Etobicoke, Ontario, M9W 5A7, Canada

ABSTRACT

We propose a novel x-ray image intensifier that incorporates the x-ray absorption, image formation and amplification stages within a simple, flat panel structure. The device, to be called the X-ray Light Valve (XLV), is based on two key components physically coupled in a sandwich structure; a solid state electrostatic x-ray detector and an electro-optic light modulator. X-ray absorption in the photoconductive detector controls the state of the electro-optic modulator via creation of charge carriers and the spatial and temporal variations that they induce in the modulator potential. Since the x-ray detector is electrostatic and the photo charge is strongly coupled to the light modulator, high resolution imaging is possible. Moreover, the amplification achieved by light modulation can avoid a coupling secondary quantum sink. Thus the XLV image may be coupled to an optical sensor, e.g. charge coupled device (CCD) camera, to produce a quantum noise limited digital radiographic imaging system. We outline the structure and the operation of the XLV. We discuss the features of the XLV based image acquisition and compare the properties of the XLV based and a phosphor screen based imaging chains.

1. INTRODUCTION

Presently most of the radiographic systems in clinical use are based on light emitting x-ray detectors, phosphor screens. Conventionally the phosphor screen image is used to expose a photographic film but in recent years there has been increasing interest in digital alternatives to film-screen radiography. Digital imaging would allow image processing, electronic transfer and storage of image data and computer aided diagnosis. Many of the proposed digital systems also rely on the use of a phosphor screen[1,2,3] and thus require conversion of light to an electronic signal. In such conversion there will always be some signal loss due to the coupling between the screen and the subsequent imaging components. When the coupling inefficiency is significant, the signal-to-noise ratio may be corrupted by the presence of a secondary quantum sink. In a modality such as x-ray imaging, in which ionizing radiation is used and x-ray exposures must be minimized to reduce the risk to the patient, such extra noise is undesirable as this prevents efficient use of x-rays.

An image intensifier introduced within the imaging chain prior to the source of the secondary quantum sink can compensate for coupling inefficiency. This paper presents a novel x-ray imaging device, the XLV, which may be used as a high resolution, flat panel image intensifier in an optically coupled system in conjunction with a CCD camera. The performance of such an imaging system ultimately depends not only on the intensifier but also on the image coupling geometry, the optical imager, digitizer and image display. In the following, we discuss the potential performance of the complete imaging system based on a high resolution, low noise and high contrast XLV. To compare the operation of the XLV based system and phosphor screen based methods, we also review optical coupling of screens to a CCD camera.

2. THE X-RAY LIGHT VALVE

The XLV combines a photoconductive x-ray detector, amorphous selenium (*a*-Se), with a liquid crystal (LC) cell light modulator in a sandwich structure as shown in Figure 1. A potential is applied across the XLV structure to create a bias electric field through the thickness of the photoconductor. When x-rays are absorbed in the photoconductor, electron-hole charge pairs are released. The applied electric field guides the charges to the opposite surfaces of the *a*-Se layer. The charges collected at the *a*-Se-LC interface cause potential variations across the LC

0-8194-1780-7/95/$6.00

cell. The potential variations give rise to changes in the orientation of the liquid crystal molecules which affects the polarization state of light from an external source propagating through the cell. The polarizers placed on either side of the structure translate the changes in light polarization to changes in light transmission. The end result is that variations in the potential in areas where x-rays are absorbed cause spatial variations in the intensity of light transmitted through the LC cell thus producing an optical representation of the x-ray image.

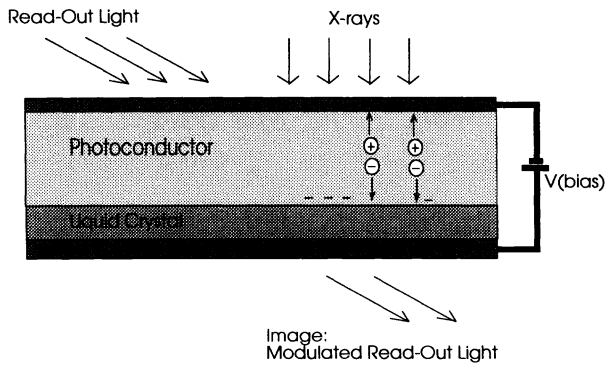

Figure 1 Structure of the XLV.

We have elsewhere[4] theoretically analyzed the properties of the XLV and have shown the XLV to be able to meet clinical radiography requirements: high resolution, x-ray quantum noise limited operation, high x-ray sensitivity, and adequate contrast over the exposure range of interest. The XLV has high resolution because: the device is not pixilated; *a*-Se is an electrostatic detector in which little image blur occurs[5]; and there will be little blurring of the signal induced electric fields in the thin (~5μm) LC cell.[6] The XLV exhibits low noise and x-ray quantum noise limited operation because it requires no external electronics (e.g. for amplification). The fundamental system noise sources are: shot noise in the photoconductor dark and bias currents; and thermal (Johnson) noise in the LC cell resistance. Sensitivity to x-rays within the clinical range for various imaging tasks is possible because: *a*-Se can be made in thick (300-500μm) layers to give high (>50%) x-ray quantum efficiency; *a*-Se provides quantum gain of 400-1000 electrons/x-ray in the diagnostic x-ray energy range; the *a*-Se signal charge is well coupled to the LC cell; and LC cells are sensitive to small potential variations. We propose to use twisted nematic LC cells which have a monotonic transmission versus potential characteristic with an operating range of few volts. By proper choice of XLV design and operating parameters, x-ray exposures within the clinical exposure range can be made to correspond to signal potentials within the operating range of the LC cell.

3. OPTICAL COUPLING OF A PHOSPHOR SCREEN

A straightforward imaging concept using a phosphor screen coupled with a lens to an optical imager such as a CCD camera is illustrated in Figure 3. This approach is currently used for portal imaging, i.e. verification of patient-beam alignment in radiation therapy with mega-voltage photons.[7]

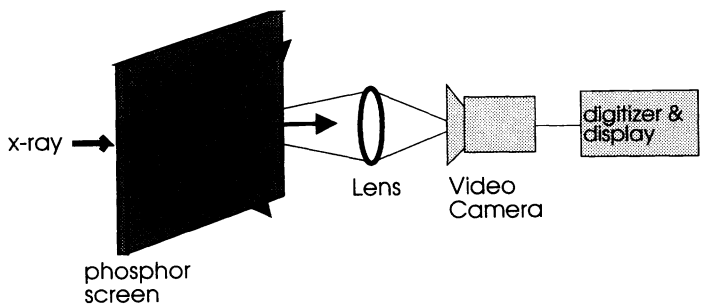

Figure 2 Lens optical coupling of a phosphor screen.

3.1. Signal and Noise

Several investigators[8,9,10] have studied the limitations of optical coupling in an x-ray imaging system by following the propagation of the signal quanta through the imaging chain. According to zero spatial frequency analysis,[11] incident monoenergetic x-rays with flux of N photons per unit area are absorbed in the detector with quantum efficiency η to produce quanta (e.g. light photons in screen). A number of quanta are released per each absorbed x-ray but only a fraction is transferred through the coupling optics and of this, only a fraction are absorbed in the optical detector to produce electronic charge. Thus the number of electrons, N_e, detected per absorbed x-ray is ηNg, where g is the total quantum gain, i.e. the number of electrons produced in the CCD for each x-ray absorbed in the phosphor screen. In the absence of system noise sources (e.g. electronic noise) the sources of noise are the x-ray quantum noise and secondary quantum (e.g. light photon) noise. Assuming these processes to be uncorrelated and governed by Poisson statistics the following signal-to-noise ratio, SNR, may be obtained:[11]

$$SNR = \frac{\sqrt{\eta N}}{\sqrt{1+\frac{1}{g}}} \qquad (1)$$

The imaging system is said to be x-ray quantum noise limited when $g>>1$ making the denominator of Equation 1 close to unity. When g decreases enough to degrade the SNR, the dominant source of noise in the system will no longer be due to the statistics of the x-ray photons. This is referred to as the presence of a secondary quantum sink. Traditionally, it has been suggested that g should equal at least 1 electron per x-ray photon (SNR loss of 30%), however spatial frequency dependent analysis[8,9] indicates that more quanta are needed to prevent a secondary quantum sink from arising at non-zero spatial frequencies due to reduction in the modulation transfer function (MTF).

Generally thousands of light photons are emitted from the screen per absorbed x-ray and CCDs are efficient (30-70%) at converting light photons to electrons. Thus the primary limit to g arises from the coupling of the fluorescent light to the CCD pixels. The efficiency of this coupling decreases with: increase in the ratio of screen size to CCD array (i.e. the demagnification); and with increase in the F-number (focal length/diameter) of the lens.[12] We may estimate the significance of the optical coupling inefficiency in clinical applications. For instance, mammography, with a 21 cm square field of view imaged with a 3 x 3 cm CCD would require a demagnification of 7. Using typical values listed by Karellas[10] for optical coupling with this demagnification, we estimate g to be ~0.3. This indicates the presence of a secondary quantum sink with a 50% loss of SNR even at zero spatial frequency.

The SNR and image quality could be improved by modification of the following parameters: increased light output from the phosphor screen; use of a wider aperture lens (which, however, has been found to lead image aberrations[7]); or decreased demagnification. The last approach has been adapted for a special small area imaging procedure for breast biopsies.[10] Increase in the optical coupling efficiency has also been proposed by coupling via reducing fiber-optic bundles.[1] Other phosphor screen based methods avoid demagnification by the use of a sufficiently large area optical detector, e.g. a photodiode array, that permits direct one-to-one coupling and completely obviates the need for a lens or a fiber-optic.[2]

3.2. Resolution

The resolution of the screen/CCD imaging system will depend on the phosphor screen, the demagnification factor, the lens, and the optical detector. Figure 3 depicts the physical process of x-ray absorption in the phosphor screen. The fluorescent light is multiply scattered within the phosphor prior to exit from the screen and this scatter leads to image blur, which increases with screen thickness. The x-ray absorption of the screen also depends on its thickness and thus there exists a tradeoff between resolution and quantum efficiency.

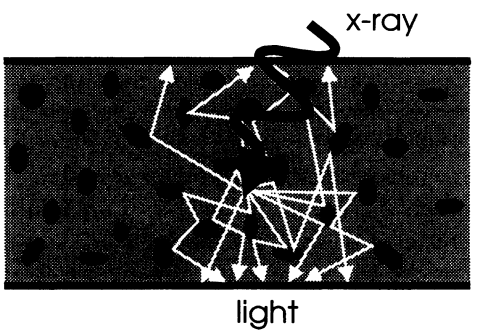

Figure 3 Signal generation in a phosphor screen.

We can obtain the modulation transfer function (MT) of the screen based imaging chain by multiplying the MTFs of the various stages. As an example consider a mammographic system based on the use of a typical phosphor screen used in film-screen mammography. A diffraction limited lens results in a negligible effect on the MT (e.g. ~85% at 200 lp/mm for a lens with a F-number= 0.7 and λ=705 nm[13]). We have assumed CCD array size and coupling geometry that would result in effective pixel size of 50μm at the screen plane. In Figure 4, we plot the MTs of a Min-R screen,[14] CCD and the product of these two, the MT of the imaging chain.

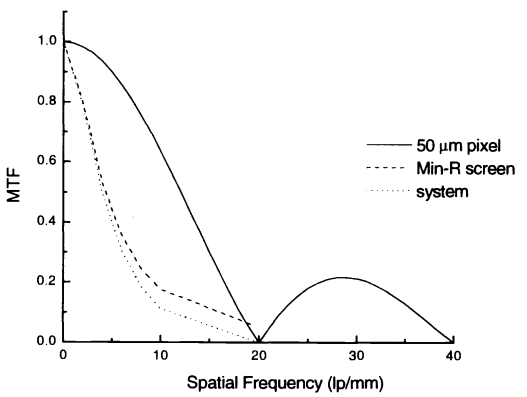

Figure 4 Modulation transfer function of CCD, Min-R screen, and the complete screen based imaging system.

4. OPTICAL COUPLING OF AN XLV

A complete imaging system, which includes the XLV coupled to an optical sensor, e.g. a CCD camera, for image capture and subsequent digitization, is illustrated in Figure 5.

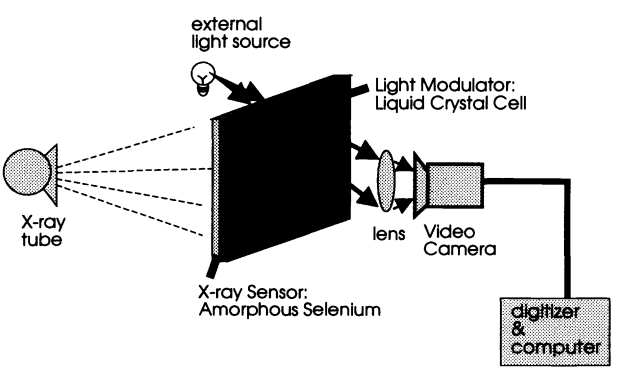

Figure 5 XLV based digital imaging chain.

4.1. Signal and Noise

The XLV is essentially an image intensifier in which the output image brightness can be controlled independently from the x-ray fluence and increased to the point where the signal at the highest expected exposure coincides with the CCD saturation. Thus the total quantum gain, g, may be defined as the ratio of the CCD full well capacity to the number of x-ray photons absorbed at the maximum exposure. On the basis of a monoenergetic x-ray beam, the number of x-rays absorbed per XLV pixel of area, A, is a product of the incident x-ray photon fluence (product of exposure, X, and the number of photons per roentgen, $N_{R(E)}$, at the specified x-ray energy E) and the quantum efficiency, which depends on the linear attenuation coefficient, μ, and thickness, d_{se}, of a-Se:

$$N_X = X N_{R(E)} A (1 - e^{\mu d_{se}}) \qquad (2)$$

We consider an XLV for chest imaging and mammography with monoenergetic beams corresponding to the approximate mean energies of commonly used x-ray spectra; 50 keV and 20 keV respectively.[15] The average exposures to the detector were taken to be 10 mR for mammography[12] and 300 μR for chest,[16] with an exposure range from 1/10 to 10 times the average exposure. An XLV with a 500 μm thick layer of a-Se could accommodate both of the above imaging tasks as the quantum efficiency would be 99.9% with 20 keV x-rays (μ=2.33 10^2 m^{-1}) and 61.3% with 50 keV x-rays (μ=1.9 10^3 m^{-1}). We take the full well capacity of the CCD to be 114,000 electrons per pixel.[10] With a 50 μm square pixel in mammography, at the maximum expected exposure (100 mR) N_X would be 1.373 10^4 photons, which corresponds to $g \sim 8.3$. For 200 μm square pixels in chest imaging, $g \sim 5.9$.

These values of g are not as high as one might expect. The reason for this is that although the XLV can be used to intensify the image by an arbitrary gain factor, the upper limit on the gain is set by saturation of the optical detector. The value of g could be increased by the use of a CCD with higher full well capacity. The same effect can be achieved with a larger number of pixels which would result in smaller pixel size. With smaller effective XLV pixel size, a smaller number of x-ray photons would be mapped to each CCD pixel which implies a greater quantum gain.

We can now determine the magnitude of the signal and the noise sources in the XLV imaging chain over the exposure ranges of interest. To do this, we assume the XLV to be x-ray quantum noise limited detector with a linear optical response and consider the signal and noise in an individual pixel. The signal is the CCD signal quanta, which at the maximum exposure coincides to the full well capacity. The x-ray quantum noise is g times the square root of the number of x-rays absorbed per pixel. The light quantum noise (which can alternatively be thought of as the CCD shot noise) is the square root of the number of signal quanta per pixel. As an example of the electronic noise, we consider a typical CCD noise (15 e^-/pixel).[10] The signal and the noise components are plotted as a function of x-ray exposure for mammography in Figure 6(a) and for chest imaging in Figure 6(b). From Figures 6(a) and 6(b) we see that the x-ray quantum noise dominates over the other components of noise for the full range of exposures (1/10 - 10 times mean exposure) required of a clinical system.

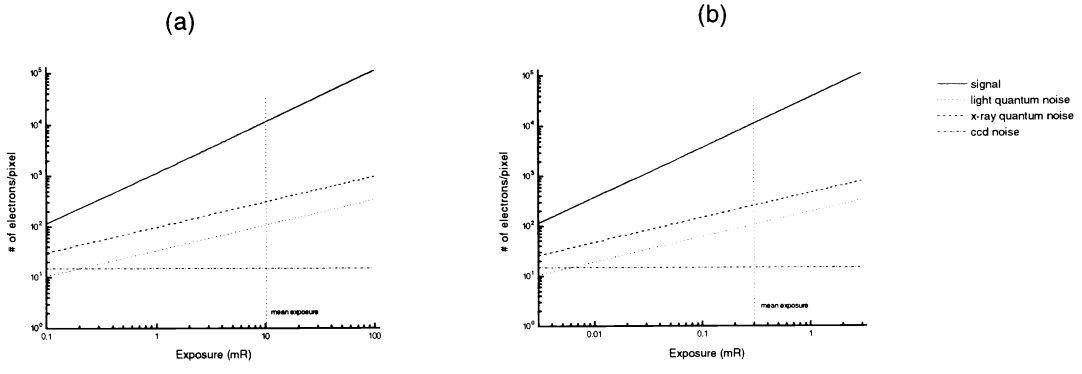

Figure 6 Signal and noise as a function of exposure in (a) mammography and (b) chest imaging.

4.2. Resolution

To investigate the resolution of the XLV based imaging system, we first consider a 2048 x 2048 pixel CCD camera. For chest imaging the area to be demagnified would be ~ 40 x 40 cm, and with such a CCD array, each pixel would be a 200 μm square. For mammography, the XLV image area would be ~ 20 cm square and a suitable pixel size[17] could be a 50 μm square. To achieve this with lens optical coupling of the whole imaging area, a high pixel count (e.g. 4000 x 4000) must be obtained by use of an improved CCD array or a mosaic of CCD arrays (e.g. 4 CCD arrays of 2048 x 2048 pixels each).

The imaging chain MT is obtained by multiplying the MTFs of the CCD and the XLV. The latter has been previously derived[4] in terms of blur in charge collection within the *a*-Se layer and the electric field spread in a two layer dielectric with an interface charge distribution. The field spread has a small effect as the LC cell is very thin (~5μm). The *a*-Se resolution is inherently very high as it is an electrostatic detector in which signal charge directly moves to the surface under the influence of an electric field as shown in Figure 7. The resolution limit in this process has been shown to be due to x-ray interactions (i.e. range of primary photoelectrons).[5]

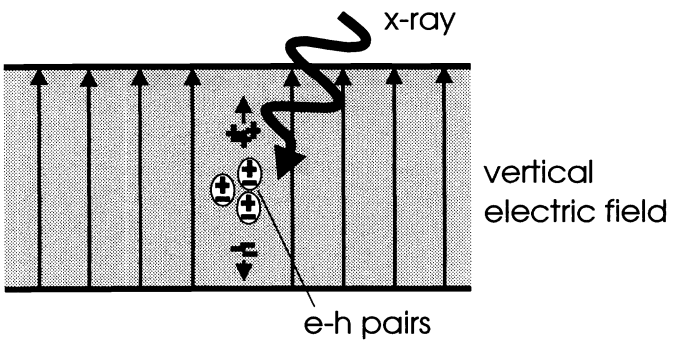

Figure 7 Signal generation in an electrostatic detector.

In Figure 8(a) we plot the MT of the CCD (for XLV pixel size of 50 μm), the previously theoretically derived MT of the XLV (at the mean energy of 20 keV), as well as their product, the complete imaging chain MT for mammography. Figure 8(b) gives the corresponding MTFs of a system for chest imaging with a 200 μm square XLV pixel and mean energy of 50 keV.

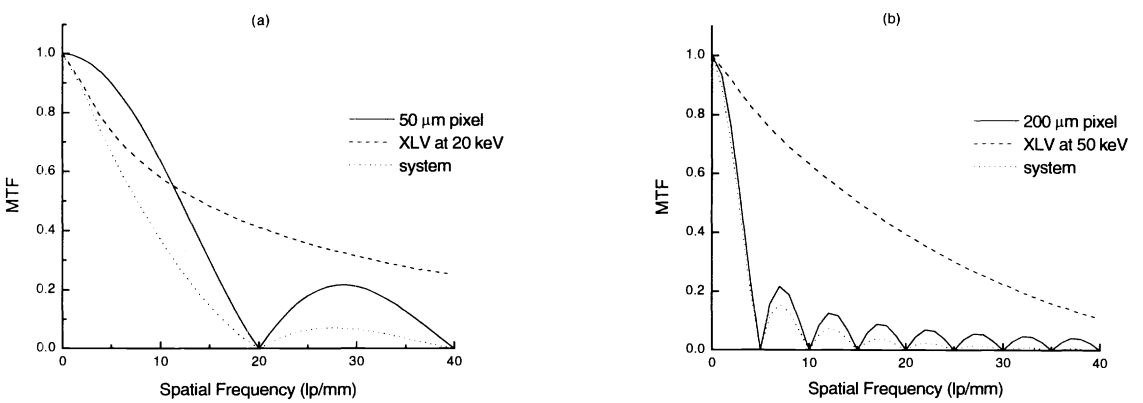

Figure 8 The modulation transfer functions of the components and the complete imaging chain in (a) mammography and (b) chest imaging.

As shown in Figures 8(a) and 8(b), the resolution of the XLV is expected to surpass that of a phosphor screen of similar quantum efficiency. Furthermore, the XLV imaging chain should have high enough resolution for

mammography, and as the resolution requirements for other imaging tasks (e.g. chest) are usually lower, we infer that the XLV imaging system has sufficient resolution for radiography in general. However, in an optically coupled system, the high resolution of the XLV and the limited optical detector sampling rate may actually lead to problems with aliasing. For example, with the above pixel sizes, Nyquist frequencies would be 10 lp/mm and 2.5 lp/mm for mammography and chest imaging respectively. To prevent aliasing, the optical detector would have to be improved to allow a larger number of pixels and thus a smaller effective pixel size.

5. EXPERIMENTAL INVESTIGATION

The experimental work on the practical feasibility of the proposed method included preliminary studies carried out with liquid crystal light valves originally designed for optical use. Such devices have been developed for applications including infrared-to-visible conversion for the military and image intensification for projection television.[18,19]

An optical light valve (OLV) with a few micrometer thick As_2Se_3 photoconductor was loaned to us by W.E.L. Haas of Xerox, Webster Research Ctr., NY. Since the device was designed for optical applications,[20,21] its x-ray quantum efficiency is very low due both high attenuation of the thick glass substrate and low attenuation in a thin photoconductor. We can expect a quantum efficiency of < 1 % at diagnostic x-ray energies. Nevertheless, we investigated x-ray imaging with the OLV using the experimental apparatus illustrated in Figure 9. This OLV has a (blue light) dielectric mirror layer between the photoconductor and the LC cell. Thus the device is operated in a reflective mode whereby the readout light is incident from the same side from which the image is viewed. The integrating sphere is used to provide uniform intensity of illumination over a field-of-view of 3 cm (while the usable imaging area of the device is ~ 5 cm square). The optical chain also includes a polarizer and an analyzer. The phantom to be imaged is placed close to the photoconductor side of the OLV in the path of the x-ray beam.

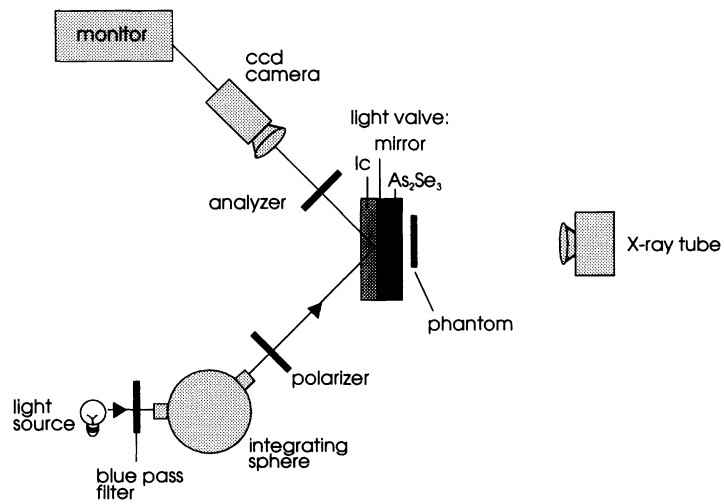

Figure 9 Experimental apparatus for x-ray imaging with the Xerox optical light valve.

Figure 10 shows an example of an x-ray image of a resolution bar pattern obtained at 100 kVp with an exposure rate of 22.5 R/sec. As the OLV was operated with a ~ 5 Hz bias potential, the exposure per frame was ~ 2.25 R. Thus a similar device with a 100% quantum efficiency would have been operational at ~ 23 mR exposure, which is within the expected clinical exposure range. The limiting resolution in the x-ray images were approximately ~ 3.5 lp/mm. In optical use considerably higher resolution had been demonstrated with similar OLVs. It is suspected that here the resolution was limited by the ordinary CCD camera used as the level of camera zooming corresponded to a Nyquist frequency of ~ 6 lp/mm in direction perpendicular to the bar pattern. The dominant source of noise in the image seemed to be the camera electronic noise (no steps had been taken to minimize this). Overall, these results were considered promising and adequate to justify further work in the design and construction of *a*-Se liquid crystal light valves optimised for x-ray imaging.

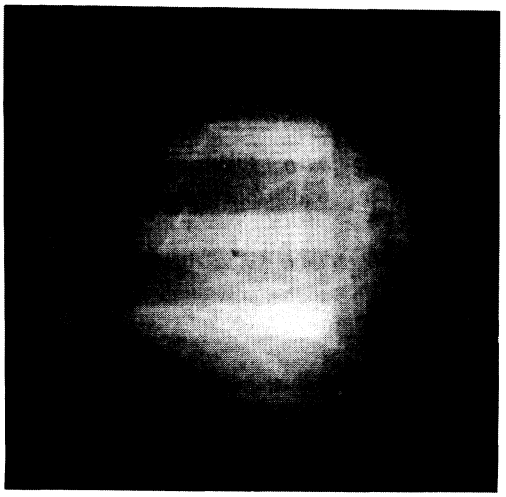

Figure 10 An x-ray image of a bar pattern obtained with the OLV.

6. SUMMARY

We have outlined the structure and operating principle of a novel imaging device, called the XLV, which may be used as a flat panel image intensifier in an optically coupled imaging chain for radiography. We have shown that, unlike phosphor screen based coupled imaging systems, optical coupling inefficiency is not an issue in the XLV imaging chain because the image brightness may be arbitrarily increased to compensate for poor coupling. However, the operation of the XLV based imaging chain may be limited by the optical detector, namely the saturation signal level and the number of pixels in the array. Initial experimental results have also been presented. The x-ray images obtained with the OLV are encouraging, and suggest that construction and characterization of an *a*-Se light valve designed specifically for radiography would be worthwhile.

7. ACKNOWLEDGEMENTS

We gratefully acknowledge invaluable assistance from Werner Haas of Xerox, Webster Research Ctr., NY, USA. We thank the Medical Research Council of Canada for financial assistance.

8. REFERENCES

1. A.D.A. Maidment, M.J. Yaffe, D.B. Plewes, G.E. Mawdsley, I.C. Soutar and B.G. Starkoski, "Imaging Performance of a Prototype Scanned-Slot Digital Mammography System", in Rodney Shaw, Ed., *Physics of Medical Imaging*, 93-103, proc. SPIE, **1896**, 1993.

2. L.E. Antonuk, J. Boudry, W. Huang, D.L. McShan, E.J. Morton, J. Yorkston, M.J. Longo, and R.A.Street, "Demonstration of megavoltage and diagnostic x-ray imaging with hydrogenated amorphous silicon arrays", Med. Phys., **19**, 1455-1466, 1992.

3. H. Kato, J. Miyahara, M. Takano, "Computed radiography with scanning laser-stimulated luminescence", in K. Doi, L. Lanzl and P-J.P. Lin, Eds., *Recent Developments in Digital Imaging, Medical Physics Monograph*, **12**, 237-263, American Institute of Physics, New York, 1984.

4. P. Rieppo and J.A. Rowlands, "X-ray Imaging with amorphous selenium: Theoretical feasibility study of implementing a liquid crystal light valve in digital radiography", (in preparation for Med. Phys.).

5. W. Que and J.A. Rowlands, "X-ray imaging with amorphous selenium: Inherent spatial resolution", Med. Phys. (in press).

6. R. M. Schaffert, *Electrophotography*, 476-511, Focal Press, London, 1980.

7. P. Munro and J.A. Rawlinson, A. Fenster, "Therapy imaging: A signal-to-noise analysis of a fluoroscopic imaging system for radiotherapy localization", Med. Phys. **17**, 763-772, 1990.

8. A.D.A Maidment and M.J. Yaffe, "Analysis of the spatial-frequency-dependent DQE of optically coupled digital mammography detectors", Med. Phys., **21**, 721-729, 1994.

9. I.A. Cunningham, M.S. Westmore and A. Fenster, "A spatial-frequency dependent quantum accounting diagram and detective quantum efficiency model of signal and noise propagation in cascaded imaging systems", Med. Phys. **21**, 417-427, 1994.

10. A. Karellas, L.J. Harris, H. Liu, M.A. Davis, and C.J. D'Orsi, "Charged coupled device detector: Performance considerations and potential for small-field mammographic imaging applications", Med. Phys., 19, 1195-1199, 1992.

11. A. Macovski, *Medical Imaging Systems*, 81-82, Prentice-Hall, Toronto, 1983.

12. W. Swindell, "The lens coupling efficiency in megavoltage imaging", Med. Phys., **18**, 1152-1153, 1991.

13. *The Melles Griot Optics Guide*, 2.4-2.6, Melles Griot, Irvine, Ca, 1990.

14. P.C. Bunch, "Detective quantum efficiency of selected mammographic screen-film combinations", in *Medical Imaging III: Image Formation*, proc. SPIE, **1090**, 67-77, 1993.

15. R. Birch, M.Marshall and G.M. Ardran in collaboration with The Hospital Physicists' Association, *Catalogue of Spectral Data For Diagnostic X-rays, Scientific Report Series No.30,* Hospital Physicists' Association, London, 1979.

16. M.M. Tesic, R.A. Mattson, G.T. Barnes, R.A. Sones and J.B. Stickney, "Digital Radiography of the Chest: Design Features and Considerations for a Prototype Unit", Radiology **148**, 259-264, 1983.

17. M.J. Yaffe,"Digital Mammography", in A.G. Haus and M.J. Yaffe, Eds., *Syllabus: A Categorical Course in Physics, Technical Aspects of Breast Imaging, 2nd Ed.*, 274, RSNA Publications, Oak Brook, Il., 1993, 274.

18. J. Grinberg, A. Jacobson, W. Bleha, L. Miller, L. Fraas, D. Boswell and G. Myer, "A new real time non-coherent to coherent light image converter - the hybrid field effect liquid crystal light valve", Opt. Eng. **14**, 217-225, 1975.

19. D. Armitage, J.I. Thackara and W.D. Eades, "Photoaddressed liquid crystal spatial light modulators," Appl. Opt. **28**, 4763-4771, 1989.

20. W.E.L. Haas, G.A. Dir, J.E. Adams and I.P. Gates, "Ultralow bias voltage image intensifiers", Appl. Phys. Letts., **29**, 631, 1976.

21. M.D. Cowen, J. Baher, T. Schmidt and W.E. Haas, "A thousand lumen real-time video", SID Digest of Technical Papers, **23**, 1992.